

# Phase retrieval and saddle-point optimization

Stefano Marchesini\*

*Lawrence Livermore National Laboratory, 7000 East Ave., Livermore, CA 94550-9234, USA and  
Center for Biophotonics Science and Technology, University of California,  
Davis, 2700 Stockton Blvd., Ste 1400, Sacramento, CA 95817, USA*

Iterative algorithms with feedback are amongst the most powerful and versatile optimization methods for phase retrieval. Among these, the hybrid input-output algorithm has demonstrated practical solutions to giga-element nonlinear phase retrieval problems, escaping local minima and producing images at resolutions beyond the capabilities of lens-based optical methods. Here, the input-output iteration is improved by a lower dimensional subspace saddle-point optimization.

© 2019 Optical Society of America

OCIS codes: 100.5070

Phase retrieval is one of the toughest challenges in optimization, requiring the solution of a large-scale nonlinear, non-convex and non-smooth constrained problem. Despite such challenge, efficient algorithms are being used in astronomical imaging, electron microscopy, lensless x-ray imaging (diffraction microscopy) and x-ray crystallography, substituting lenses and other optical elements in the image-forming process.

In diffraction microscopy, photons scattered from an object (diffraction pattern) are recombined by computational methods. X-ray diffraction microscopy<sup>1</sup> has successfully been applied to image objects as complex as biological cells<sup>2</sup>, quantum dots<sup>3</sup>, nanocrystals<sup>4</sup>, nanoscale aerogel structures<sup>5</sup>. Nanofabricated test objects were reconstructed computationally in 3D with several millions of 10 nm resolution elements<sup>6</sup>, other test patterns were captured in the fastest flash image ever recorded at sub-optical resolution<sup>7</sup>.

These experimental methods (see e.g.<sup>8</sup> for a review) are being developed thanks to advances in optimization techniques, primarily the introduction of a control-feedback method proposed by Fienup (Hybrid Input Output-HIO<sup>9,10</sup>).

The important theoretical insight that these iterations may be viewed as projections in Hilbert space<sup>11,12</sup> has allowed theoreticians to analyze and improve on the basic HIO algorithm<sup>13,14,15,16</sup>. More recently Elser et al.<sup>17</sup> pointed out that the Difference Map algorithm, derived from HIO, can be applied to problems as various as graph coloring, protein folding and sudoku.

The algorithm proposed here is based on a reformulation of the original HIO algorithm from a gradient-based optimization perspective. This algorithm optimizes conflicting requirements of fitting the data and satisfying the constraints, by seeking the saddle-point of the difference

between antagonistic error metrics<sup>18</sup>. Here, each input-output iteration is improved by a lower dimensional subspace optimization of this saddle-point problem. This lower dimensional optimization (performed here by Newton methods), is conceptually the same as the one dimensional line search of gradient based methods, used to avoid overshooting and undershooting in new search directions and providing faster and more reliable algorithms. Here, the lower dimensional optimization is performed along the steepest descent-ascent directions defined by the constraints.

The first Sections introduce the saddle point optimization method, reformulating the HIO algorithm in terms of gradients and constraints (see<sup>18</sup> for further details). Sections 4 and 5 describe this lower dimensional optimization method and benchmarking results.

## 1. Phase retrieval problem

When we record the diffraction pattern intensity of light scattered by an object, the phase information is lost. Apart from normalization factors, an object with density  $\rho(\mathbf{r})$ ,  $\mathbf{r}$  being the coordinates in the *object* (or *real*) space, generates a diffraction pattern intensity equal to the modulus square of the Fourier Transform (FT)  $\tilde{\rho}(\mathbf{k})$ :

$$I(\mathbf{k}) = |\tilde{\rho}(\mathbf{k})|^2 \quad (1)$$

where  $\mathbf{k}$  represent the coordinate in the Fourier (or Reciprocal) space. In absence of constraints, any phase  $\varphi(\mathbf{k})$  can be applied to form our solution  $\tilde{\rho} = \sqrt{I}e^{i\varphi}$ .

Phase retrieval consists in solving (Eq. 1) from the measured intensity values  $I(\mathbf{k})$  and some other prior knowledge (constraints). For example, the simple knowledge that the density is a nonnegative function is often sufficient to re-image a diffracting object on a screen. However, even this constraint is not always available in practical experiments, where the object interacts by absorbing as well as refracting incident light, and the often missing 0-frequency information reduces the scope of such constraint introducing a variable baseline. The

\*Current address: Lawrence Berkeley National Laboratory, 1 Cyclotron Rd, Berkeley CA 94720, USA. e-mail: smarchesini@lbl.gov

problem is generalized in the rest of the article to the most complex case of objects with complex “density”.

Diffraction microscopy solves the phase problem using the knowledge that the object being imaged is isolated, it is assumed to be 0 outside a region called support  $S$ :

$$\rho(\mathbf{r}) = 0, \text{ if } \mathbf{r} \notin S. \quad (2)$$

In case of complex objects, this region is the only constraint and needs to be well defined, tightly wrapping the object. In many cases sharp objects or illuminating beam boundaries are sufficient to obtain a tight support of the object *ab-initio*<sup>6,19</sup>.

A projection onto this set ( $\mathbf{P}_s$ ) involves setting to 0 the components outside the support, while leaving the rest of the values unchanged (Fig. 1(a)):

$$\mathbf{P}_s \rho(\mathbf{r}) = \begin{cases} \rho(\mathbf{r}) & \text{if } \mathbf{r} \in S, \\ 0 & \text{otherwise.} \end{cases} \quad (3)$$

Its complementary projector can be expressed as  $\mathbf{P}_{\bar{s}} = \mathbf{I} - \mathbf{P}_s$ .

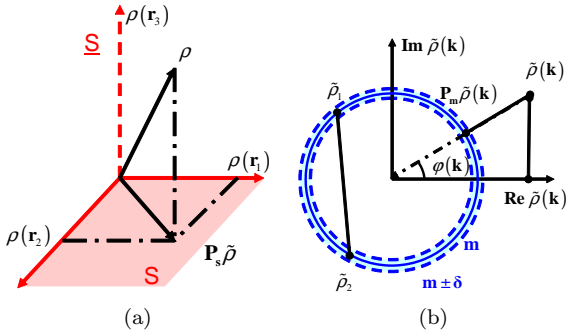


Fig. 1. Examples of sets and projectors: (a) Support: The axes represent the values on 3 pixels of an image  $\rho$  known to be 0 outside the support. The vertical axis  $\rho(\mathbf{r}_3)$  represents a pixel outside the support ( $\mathbf{r}_3 \in \bar{S}$ ), while the horizontal plane represents pixels inside the support  $S$ . The projection on this set is performed simply by setting to 0 all the pixels outside the support. (b) Modulus: A pixel (in Fourier space) with a given complex value is projected on the closest point on the circle defined by the radius  $m$ . If there is some uncertainty in the value of the radius  $m \pm \delta$ , the circle becomes a band. The circle is a non-convex set, since the linear combination between two points on the same set,  $\rho_1$  and  $\rho_2$  does not lie on the set. Also represented in the figure is the projection on the real axis (reality projection)<sup>18</sup>.

The projection to the nearest solution of (Eq. 1) in reciprocal space is obtained by setting the modulus to the measured one  $m(\mathbf{k}) = \sqrt{I(\mathbf{k})}$ , and leaving the phase unchanged (Fig. 1(b)):

$$\tilde{\mathbf{P}}_m \tilde{\rho}(\mathbf{k}) = \tilde{\mathbf{P}}_m |\tilde{\rho}(\mathbf{k})| e^{i\varphi(\mathbf{k})} = \sqrt{I(\mathbf{k})} e^{i\varphi(\mathbf{k})}, \quad (4)$$

Singularities arise when  $\rho$  is close to 0, and a small change in its value will project on a distant point. Such projector is a “diagonal” operator in Fourier space, acting element-by-element on each amplitude. When applied to real-space densities  $\rho(\mathbf{r})$ , it becomes non-local, mixing every element with a forward  $\mathcal{F}$  and inverse  $\mathcal{F}^{-1}$  Fourier transform:

$$\mathbf{P}_m = \mathcal{F}^{-1} \tilde{\mathbf{P}}_m \mathcal{F}. \quad (5)$$

The Euclidean length  $\|\rho\|$  of a vector  $\rho$  is defined as:

$$\|\rho\|^2 = \rho^\dagger \cdot \rho = \sum_{\mathbf{r}} |\rho(\mathbf{r})|^2 = \sum_{\mathbf{k}} |\tilde{\rho}(\mathbf{k})|^2. \quad (6)$$

If some noise  $\sigma(k)$  is present, the sum should be weighted by  $w = \frac{1}{\sigma^2}$ . The distance from the current point to the corresponding set  $\|\mathbf{P}\rho - \rho\|$  is the basis for our error metric:

$$\begin{aligned} \varepsilon_s(\rho) &= \|\mathbf{P}_s \rho - \rho\|, \\ \varepsilon_m(\rho) &= \|\mathbf{P}_m \rho - \rho\|, \end{aligned} \quad (7)$$

or their normalized version  $\bar{\varepsilon}_{s,m}(\rho) = \frac{\varepsilon_{s,m}(\rho)}{\|\mathbf{P}_{s,m}\rho\|}$ .

The gradients of the squared error metrics can be expressed in terms of projectors<sup>10,20</sup>:

$$\nabla \varepsilon_m^2(\rho) = -2[\mathbf{P}_m - \mathbf{I}]\rho \quad (8)$$

$$\nabla \varepsilon_s^2(\rho) = -2[\mathbf{P}_s - \mathbf{I}]\rho, \quad (9)$$

Steps of  $-\frac{1}{2}\nabla \varepsilon_{s,m}^2$  bring the corresponding error metrics to 0. The solution, hopefully unique, is obtained when both error metrics are 0.

## 2. Minimization in feasible space

One popular algorithm<sup>10,21</sup> minimizes the error metric  $\varepsilon_m(\rho)$ :

$$\begin{aligned} \min_{\rho} \varepsilon_m^2(\rho), \\ \text{subject to } \mathbf{P}_s \rho = 0, \end{aligned} \quad (10)$$

by enforcing the constraint and moving only in the feasible space  $\rho_s = \mathbf{P}_s \rho$ . The problem is transformed into an unconstrained optimization with a reduced set of variables  $\rho_s$ :

$$\min_{\rho_s} \varepsilon_m^2(\rho_s). \quad (11)$$

The steepest descent direction is projected in the feasible space:

$$\begin{aligned} \rho^{(n+1)} &= \rho^{(n)} + \Delta \rho^{(n)}, \\ \Delta \rho^{(n)} &= -\frac{1}{2} \nabla_s \varepsilon_m^2(\rho^{(n)}), \\ &= -\mathbf{P}_s [\mathbf{I} - \mathbf{P}_m] \rho^{(n)}, \end{aligned} \quad (12)$$

where  $\nabla_s = \mathbf{P}_s \nabla$  is the component of the gradient in the support. Notice that a step of  $-\frac{1}{2}\nabla \varepsilon_m^2(\rho)$  brings

the error  $\varepsilon_m^2(\rho)$  to 0. By projecting this step, setting to 0 some of its components, we reduce the step length. Typically (within a linear approximation) the optimal step is longer than this step, we can move along this direction and minimize further the error metric.

This algorithm is usually written as a projection algorithm:

$$\begin{aligned}\rho^{(n+1)} &= \rho^{(n)} + \Delta\rho^{(n)}, \\ &= \mathbf{P}_s \mathbf{P}_m \rho^{(n)}.\end{aligned}\quad (13)$$

By projecting back and forth between two sets, it converges to the local minimum. Such algorithm is commonly referred to as Error Reduction (ER) in the phase retrieval community.

The simplest acceleration strategy, the steepest descent method, performs a line search of the local minimum in the steepest descent direction:

$$\min_{\delta} \varepsilon_m^2(\rho + \delta \Delta\rho). \quad (14)$$

At a minimum any further movement in the direction of the current step increases the error metric; the gradient direction must be perpendicular to the current step. In the steepest descent case, where the step is proportional to the gradient, the current step and the next become orthogonal:

$$\begin{aligned}\frac{\partial}{\partial \delta} \varepsilon_m^2(\rho + \delta \Delta\rho) &= \langle \Delta\rho | \mathbf{P}_s [\mathbf{I} - \mathbf{P}_m] (\rho + \delta \Delta\rho_s) \rangle_r, \\ 0 &= \langle \Delta\rho_s | [\mathbf{I} - \mathbf{P}_m] (\rho + \delta \Delta\rho_s) \rangle_r,\end{aligned}\quad (15)$$

where  $\langle \mathbf{x} | \mathbf{y} \rangle_r = \Re(\mathbf{x}^\dagger \cdot \mathbf{y})$ . The line search algorithm can use  $\varepsilon_m^2$ , and/or its derivative in (Eq. 15). This optimization should be performed in reciprocal space, where the modulus projector is fast to compute (Eq. (4)), while the support projection requires two Fourier transforms:

$$\tilde{\mathbf{P}}_s = \mathcal{F} \mathbf{P}_s \mathcal{F}^{-1}, \quad (16)$$

but it needs to be computed once to calculate  $\Delta\rho_s$ .

The steepest descent method is known to be inefficient in the presence of long narrow valleys, where imposing that successive steps be perpendicular causes the algorithm to zig-zag down the valley. This problem is solved by the non-linear conjugate gradient method<sup>22,23,24,25,26</sup>.

### 3. Saddle-point optimization

The following algorithm is a reformulation of the HIO algorithm from a gradient/constraint perspective. We seek the saddle point of the error-metric difference  $\mathcal{L}(\rho) = \varepsilon_m^2(\rho) - \varepsilon_s^2(\rho)$ <sup>18</sup>:

$$\min_{\rho_s} \max_{\rho_{\underline{s}}} \mathcal{L}(\rho_s + \rho_{\underline{s}}). \quad (17)$$

Using equations (8) and (9) we obtain the gradient:

$$\nabla \mathcal{L}(\rho) = 2[\mathbf{P}_s - \mathbf{P}_m]\rho. \quad (18)$$

Since we seek the saddle point, the step direction has to go in the descent direction for  $\rho_s$  ( $-\mathbf{P}_s \nabla$ ) and ascent direction ( $+\mathbf{P}_{\underline{s}} \nabla$ ) for  $\rho_{\underline{s}}$ . For reasons discussed in appendix, we reduce the  $\mathbf{P}_{\underline{s}}$  component by a relaxation parameter  $\bar{\beta} \in [0.5, 1]$ :

$$\Delta\rho^{(n)} = \{-\mathbf{P}_s + \bar{\beta} \mathbf{P}_{\underline{s}}\} \frac{1}{2} \nabla \mathcal{L}(\rho^{(n)}). \quad (19)$$

Using the gradient in Eq. 18 and the relation  $\mathbf{P}_{\underline{s}} \mathbf{P}_s = \mathbf{0}$ , we can express the step and the new iteration point  $\rho^{(n+1)}$  as:

$$\begin{aligned}\Delta\rho^{(n)} &= \{\mathbf{P}_s[\mathbf{P}_m - \mathbf{I}] - \bar{\beta} \mathbf{P}_{\underline{s}} \mathbf{P}_m\} \rho^{(n)}, \\ \rho^{(n+1)} &= [\mathbf{P}_s \mathbf{P}_m + \mathbf{P}_{\underline{s}}[\mathbf{I} - \bar{\beta} \mathbf{P}_m]] \rho^{(n)}.\end{aligned}\quad (20)$$

The new iteration can be expressed in a more familiar form of the HIO algorithm<sup>9,10</sup>:

$$\rho^{(n+1)}(\mathbf{r}) = \begin{cases} \mathbf{P}_m \rho^{(n)}(\mathbf{r}) & \text{if } \mathbf{r} \in S, \\ (\mathbf{I} - \bar{\beta} \mathbf{P}_m) \rho^{(n)}(\mathbf{r}) & \text{otherwise.} \end{cases} \quad (21)$$

Rather than setting to 0 the object  $\rho(\mathbf{r})$  where it is known to be 0 ( $\mathbf{r} \notin S$ ), this algorithm seeks a stable condition of a feedback system in which the nonlinear operator  $\mathbf{P}_m$  provides the feedback term  $\mathbf{P}_{\underline{s}} \mathbf{P}_m \rho$ . From a fixed point<sup>13</sup> whereby the feedback is 0 but the constraint is violated ( $\mathbf{P}_{\underline{s}} \rho \neq 0$ ) it is often possible to obtain a solution by a simple projection  $\mathbf{P}_m \rho$ . In fact  $\mathbf{P}_m \rho$  often satisfies the constraints better than the current iteration  $\rho$ , as the algorithm tries to escape a local minimum.

In the steepest descent method, optimization of the step length is obtained by increasing a multiplication factor  $\delta$  until the current and next search directions become perpendicular to one another:

$$\langle \Delta\rho | [-\mathbf{P}_s + \bar{\beta} \mathbf{P}_{\underline{s}}] \nabla \mathcal{L}(\rho + \delta \Delta\rho) \rangle_r = 0. \quad (22)$$

A more robust strategy involves replacing the one dimensional search with a two dimensional optimization of the saddle point:

$$\begin{aligned}\min_{\alpha} \max_{\beta} \psi(\alpha, \beta), \\ \psi(\alpha, \beta) &= \mathcal{L}(\rho + \alpha \Delta\rho_s + \beta \Delta\rho_{\underline{s}}), \\ \Delta\rho_s &= -\frac{1}{2} \nabla_s \mathcal{L}(\rho); \Delta\rho_{\underline{s}} = \frac{1}{2} \nabla_{\underline{s}} \mathcal{L}(\rho);\end{aligned}\quad (23)$$

where both components ( $\mathbf{P}_s, \mathbf{P}_{\underline{s}}$ ) of successive steps are perpendicular to one another:

$$\begin{aligned}\frac{\partial \psi}{\partial \alpha} &= \langle \Delta\rho_s | \nabla \mathcal{L}(\rho + \alpha \Delta\rho_s + \beta \Delta\rho_{\underline{s}}) \rangle_r = 0, \\ \frac{\partial \psi}{\partial \beta} &= \langle \Delta\rho_{\underline{s}} | \nabla \mathcal{L}(\rho + \alpha \Delta\rho_s + \beta \Delta\rho_{\underline{s}}) \rangle_r = 0.\end{aligned}\quad (25)$$

This two dimensional minmax problem needs to be fast to provide real acceleration and will be discussed in the following section.

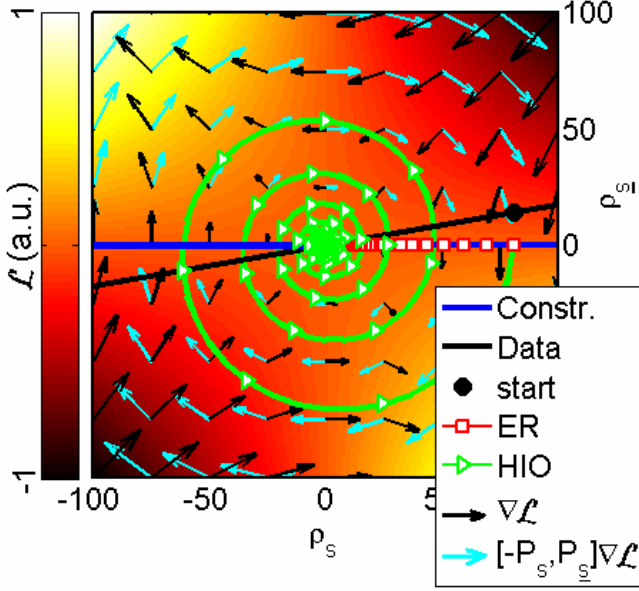


Fig. 2. Algorithms seek the intersection between two sets (data and constraints represented by two lines) in different ways: ER projects back and forth between the two sets, moving within the constraint (horizontal line). HIO seeks the saddle point ( $\min_s \max_s$ ) of ( $\mathcal{L}$ ), represented in background in pseudocolormap.  $\mathcal{L}$  is the difference of the square distances ( $\varepsilon^2$ ) between the current point and the two sets. The gradient ( $\nabla \mathcal{L}$ ) is indicated by black arrows. In order to reach the saddle point, HIO spirals toward the solution by inverting the gradient component parallel to the constraint (horizontal direction) following a descent-ascent direction ( $[-P_s + P_{\underline{s}}] \nabla \mathcal{L}$ ) toward the solution.

#### 4. Two dimensional subproblem

The local saddle point (Eq. 24) requires two conditions to be met. The first order condition is that the solution is a stationary point, where the gradient of  $\psi$  is 0 (Eq. 25). We rewrite the condition in a compact form:

$$\nabla_{\tau} \psi(\tau) = \langle \Delta \rho | \nabla_{\rho} \mathcal{L}(\rho + \tau^T \Delta \rho) \rangle_{\tau} = 0, \quad (26)$$

$$\tau = \begin{pmatrix} \alpha \\ \beta \end{pmatrix}, \Delta \rho = \begin{pmatrix} \Delta \rho_s \\ \Delta \rho_{\underline{s}} \end{pmatrix}, \nabla_{\rho} = \begin{pmatrix} \nabla_s \\ \nabla_{\underline{s}} \end{pmatrix}. \quad (27)$$

At the origin ( $\tau = 0$ ), the gradient  $\nabla_{\tau} \psi$  is descending in the  $P_s$  subspace and ascending in the  $P_{\underline{s}}$  subspace:

$$\begin{aligned} \nabla_{\tau} \psi(0) &= \begin{pmatrix} \Delta \rho_s | \nabla_s \mathcal{L}(\rho) \\ \Delta \rho_{\underline{s}} | \nabla_{\underline{s}} \mathcal{L}(\rho) \end{pmatrix}, \\ &= \frac{1}{2} \begin{pmatrix} -||\Delta \rho_s||^2 \\ +||\Delta \rho_{\underline{s}}||^2 \end{pmatrix} = 2 \begin{pmatrix} -||\nabla_s \mathcal{L}(\rho)||^2 \\ +||\nabla_{\underline{s}} \mathcal{L}(\rho)||^2 \end{pmatrix}, \end{aligned} \quad (28)$$

Second order conditions (min-max) require the Hessian  $\mathcal{H}$  of  $\psi$  (the Jacobian of (Eq. 26)) to be symmetric and indefinite (neither positive nor negative definite):

$$\mathcal{H}_{\tau} = \begin{pmatrix} \partial_{\alpha} \partial_{\alpha} & \partial_{\alpha} \partial_{\beta} \\ \partial_{\beta} \partial_{\alpha} & \partial_{\beta} \partial_{\beta} \end{pmatrix} \psi, \begin{cases} \mathcal{H}_{\alpha, \alpha} \geq 0, \\ \mathcal{H}_{\beta, \beta} \leq 0. \end{cases} \quad (29)$$

This Hessian is computed analytically (see appendix), it is small ( $2 \times 2$ ), and can be used to compute the Newton step:

$$\Delta \tau = -\mathcal{H}^{-1} \nabla_{\tau} \psi. \quad (30)$$

However, the Hessian precise value is not necessary and requires an effort that could be avoided by other methods. The minimal residual method optimizes the norm of the gradient:

$$\min_{\tau} \Phi(\tau), \quad \Phi = \frac{1}{2} ||\nabla_{\tau} \psi(\tau)||^2, \quad (31)$$

transforming the saddle point problem in a minimization problem, and providing the metric  $\Phi$  to monitor progress. However by minimizing the norm of the gradients, we decrease the condition number, and can move to other stationary points and the algorithm becomes less robust.

The normalized steepest descent-ascent direction can be expressed using an approximate diagonal Hessian whose elements are equal to  $-\nabla \psi(0)$ :

$$\hat{\mathcal{H}}^{SDA} = 2 \begin{pmatrix} ||\Delta \rho_s||^2 & 0 \\ 0 & -||\Delta \rho_{\underline{s}}||^2 \end{pmatrix}. \quad (32)$$

The Hessians  $\hat{\mathcal{H}}$  satisfies condition (Eq. (29)), ensuring that  $\Delta \tau$  is less than  $90^\circ$  from the direction of the saddle. Starting from  $\tau^{(0)} = \mathbf{0}$ , the first iteration gives a unit step  $\tau^{(1)} = -\hat{\mathcal{H}}^{-1} \nabla \psi(\mathbf{0}) = \begin{pmatrix} 1 \\ 1/\beta \end{pmatrix}$ . A preconditioner can be used to reduce the feedback:

$$\hat{\mathcal{H}}^{HIO} = \begin{pmatrix} 1 & 0 \\ 0 & 1/\beta \end{pmatrix} \hat{\mathcal{H}}^{SDA}, \quad (33)$$

providing the HIO step at the first iteration,  $\tau^{(1)} = \begin{pmatrix} 1 \\ \beta \end{pmatrix}$ . This approximate Hessian can be used as a starting guess, which is often all it is needed to achieve fast convergence.

We can perform a line search using the preconditioner  $\hat{\mathcal{H}}^{-1}$ :

$$\langle \Delta \tau | \hat{\mathcal{H}}^{-1} \nabla_{\tau} \psi(\tau + \delta \Delta \tau) \rangle_{\tau} = 0. \quad (34)$$

However the Hessian of  $\hat{\mathcal{H}}^{-1} \psi$  is antisymmetric, the algorithm is unstable and could spiral away from the solution. The bi-conjugate gradient method applies to symmetric indefinite Hessians and monitors progress of the algorithm. Conjugate directions  $\Lambda \tau$  replace the steepest descent direction in the line search:

$$\Lambda \tau^{(n+1)} = \Delta \tau^{(n+1)} + \gamma^{(n)} \Lambda \tau^{(n)}, \quad (35)$$

$$\gamma^{(n)} = \frac{\langle \Delta \tau^{(n+1)} | \hat{\mathcal{H}}^{(-1)} (\nabla \psi(\tau^{(n+1)}) - \nabla \psi(\tau^{(n)})) \rangle}{\langle \Delta \tau^{(n)} | \hat{\mathcal{H}}^{-1} \Delta \nabla \psi(\tau^{(n)}) \rangle}.$$

A better option is to use a quasi-Newton update of the Hessian (a secant method in higher dimension) based on the new gradient values. The *Symmetric Rank 1* method can be applied to indefinite problems<sup>27</sup>:

$$\begin{aligned} \mathbf{y} &= \nabla_{\tau} \psi(\tau + \Delta \tau) - \nabla_{\tau} \psi(\tau), \\ \Delta \mathcal{H}^{-1} &= \frac{||\Delta \tau - \mathcal{H}^{-1} \mathbf{y}||^2}{(\Delta \tau - \mathcal{H}^{-1} \mathbf{y})^T \cdot \mathbf{y}}, \\ \mathcal{H}^{-1} &\rightarrow \mathcal{H}^{-1} + \Delta \mathcal{H}^{-1}. \end{aligned} \quad (36)$$

Second order conditions (Eq. 29) can be imposed to the Hessian, by flipping the sign or setting to 0 the values that violate them.  $\Phi$  can be used to monitor progress, as long as we are in the neighborhood of the solution and the Hessian satisfies second order conditions (Eq. 29). It was found that the Hessian and step size parameters were fairly constant for each 2D optimization, therefore the first guess for  $\tau$  and  $\mathcal{H}$  was obtained from the average of the previous 5 of such optimizations. With such initial guess, 3 SR1 iterations of the lower dimensional problem were often sufficient to reduce  $\Phi$  below a threshold of 0.01  $\Phi(0)$  in the tests described below.

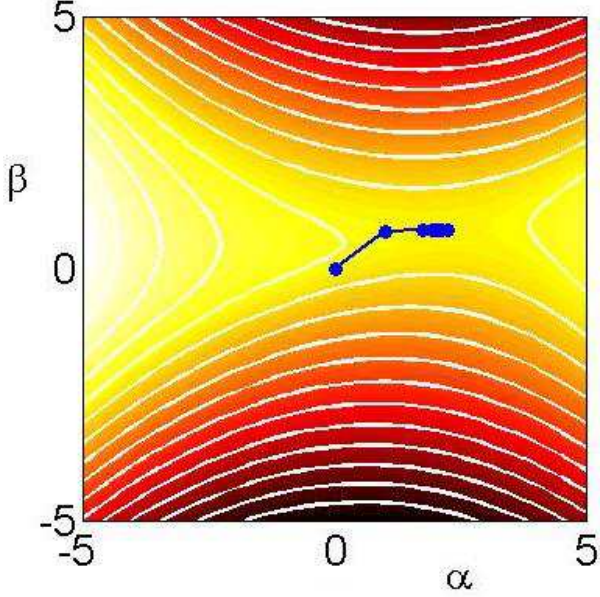


Fig. 3. Pseudocolor and contour maps of  $\psi(\alpha, \beta)$  are depicted in the background. This  $\psi$  was computed from one iteration of the test described in Sec. 5. The saddle, typical of this test, was wider in the horizontal direction, and narrower in the vertical, showing the importance of the relaxation parameter  $\bar{\beta} < 1$  to reduce (precondition) the vertical move. However, the condition number increased near the saddle-point as it became narrower in the vertical direction. Often the dependence of  $\psi$  with respect to the fitting parameter  $\beta$  (vertical axis) resembled a v centered near the solution, and successive iterations using just a preconditioner and not line search often jumped back and forth near the saddle-point. Iterations to the 2D saddle point using the SR1 update of the Hessian are shown in blue.

In summary, an efficient algorithm is obtained by a combination of HIO/quasi-Newton/Newton methods with a trust region  $|\Delta\tau| \leq r$ :

1. calculate step  $\Delta\rho = -\frac{1}{2} \begin{pmatrix} \nabla_s \mathcal{L} \\ -\nabla_a \mathcal{L} \end{pmatrix}$ , and set trust region radius  $r = r_{\max}$ .
2. if the iteration number is  $\leq 5$ , use HIO as first guess:  $\mathcal{H} = \hat{\mathcal{H}}$ ,  $\tau = (1, \bar{\beta})$ .

3. otherwise average 5 previous optimized step sizes  $\tau$ , and Hessians  $\mathcal{H}$ , and use the average as initial guess.
4. calculate gradient  $\nabla\psi(\tau)$ . If small, exit loop (go to 10).
5. compute Newton step using approximate Hessian:  $\Delta\tau = -\mathcal{H}^{-1}\nabla\psi$ , enforce trust region  $|\Delta\tau| < r$ .
6. update Hessian with SR1 method (Eq. 36).
7. if the Hessian error  $\|\Delta\tau - \mathcal{H}^{-1}y\|^2$  is too large, calculate the true Hessian, perform a line search, decrease trust region radius  $r$ .
8. force Hessian to satisfy second order conditions (Eq. 29), by changing the sign of the values that violate conditions.
9. update  $\tau \rightarrow \tau + \Delta\tau$  and go back to 4.
10. update  $\rho \rightarrow \rho + \tau^T \Delta\rho$ , and go back to 1.

The trust region is used to obtain a more robust algorithm, is reset at each inner loop, it increases if things are going well, decreases if the iteration is having trouble, but it is kept between  $(r_{\min}, r_{\max})$ , typically  $(0.5, 3)$ . We can keep track of  $\tau, \nabla\tau$  computed, and restart the algorithm once in a while from the root of the 2D linear fit of  $\nabla\psi(\tau)$ .

We can easily extend this algorithm to two successive steepest descent-ascent directions, by performing a higher dimensional saddle-point optimization:

$$\min_{\alpha^{(n,n+1)}} \max_{\beta^{(n,n+1)}} \mathcal{L} \left( \rho + \tau^{(n+1)} \Delta\rho^{(n+1)} + \tau^{(n)} \Delta\rho^{(n)} \right)$$

The 4D optimization is performed using the same Newton/quasi-Newton trust-region optimization as in the 2D case.

## 5. Performance tests

The tests presented here were combined with other algorithms in<sup>18</sup>. In such comparison between algorithms, the origin HIO algorithm performed better than other algorithms described in the literature. Fig. 4 was used to simulate a diffraction pattern, and several phase retrieval tests were performed using different random starts. When applying a nonnegativity constraint HIO always converged within a few hundred iterations. To test the algorithms with a more difficult problem, non-negativity and reality constraints were removed, allowing the reconstructed image to be complex, adding many degrees of freedom within the constraint.

When the error metric  $\varepsilon_m$  fell below a threshold it was considered a successful reconstruction. The threshold  $10^{-4}$  chosen was enough to obtain a visually good reconstructions.





Fig. 4. Test figure used for benchmarking (total size:  $256^2$ , object size:  $128^2$  pixels. The support was slightly larger than the object:  $129^2$  pixels).

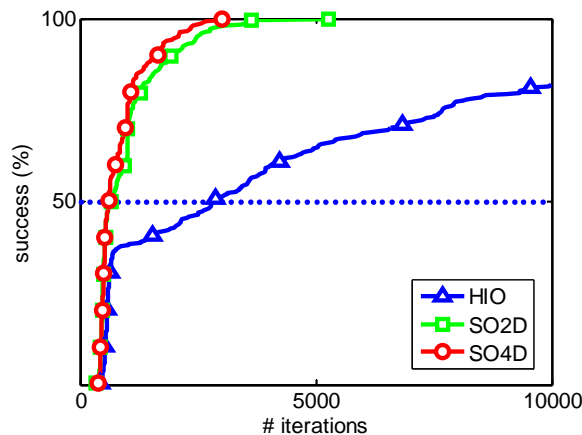


Fig. 5. Successful phase retrievals, starting from random phases, as a function of iterations. When the normalized error metric  $\bar{\epsilon}_m$  falls below a threshold ( $10^{-4}$ ) it is considered a Successful reconstruction. The plot represents the cumulative sum of the number of Successful reconstructions vs the number of iterations. Comparison with other algorithms is shown in<sup>18</sup>.

Fig. 5 shows the relative performance of the various algorithms. By adding 2D or 4D optimization, the algorithm converged more reliably and in less iterations to a solution (Table 1). The 2D (and 4D) optimization, written in a slower upper-level language (matlab) increased the computational time of each iteration by a factor of 2 (and 3) and required the storage 2 (and 4) additional matrices compared to HIO. HIO itself requires 2 matrices in addition to the data and constraints).

This lower dimensional optimization employs matrix cross products, computing a number of floating point operations proportional to the number of elements of the images. The Fourier transforms employed to calculate the steps in the higher dimensional problem will dominate the computational burden for larger matrices.

Table 1. Benchmark of various algorithms (250 trials).

Algorithm	No. of iterations for		success rate (total)
	50% success	100% success	
HIO	2790	> 10000	82%
SO2D	656	5259	100%
SO4D	605	2999	100%

## 6. Conclusions

The hybrid input-output method, usually described as a projection algorithm, is a truly remarkable method to solve the phase problem. Elser, with his own projection algorithm, has shown that the scope of these methods is surprisingly broad, with applications as diverse as protein folding and Sudoku<sup>17</sup>.

When written as a saddle point problem, HIO speed and reliability can be improved by applying Newton methods to explore a lower dimensional search direction.

This approach differs from other nonlinear optimization algorithms that try to satisfy constraints using various forms of barriers or trust regions, often falling in the first local minimum, requiring stochastic methods to climb out. The saddle-point algorithm, while following a path indicated by a gradient, does not seek a minimum and does not stop at local minima. Although stagnation occurs, it appears that the area of convergence to the global solution is much larger compared to simple minimization methods. Problems arise at the locations of 0 intensity values where phase singularities occur. Various forms of preconditioning could be applied to overcome this problem. An intriguing method has been suggested by Oszlányi and Sütö<sup>28</sup> whereby the phases of weak intensities are rotated  $90^\circ$ .

In this paper the saddle-point optimization was performed for a simple equality constraint  $\mathbf{P}_s \rho = 0$ . Such linear constraint allows rapid calculation of the gradients involved in the lower dimensional optimization. A linear approximation of the constraint, or more advanced trust region methods could be applied to inequalities and other nonlinear constraints such as thresholds, histograms, atomicity and object connectivity.

The relationship between projections and gradients can be used to obtain one from the other within a linear approximation. This saddle-point optimization formalism can easily be generalized to other problems of conflicting requirements where gradients or projections can be computed.

## Acknowledgments

This work was performed under the auspices of the U.S. Department of Energy by the Lawrence Livermore National Laboratory under Contract No. W-7405-ENG-48 and the Director, Office of Energy Research. This work was partially funded by the National Science Foundation through the Center for Biophotonics, University

of California, Davis, under Cooperative Agreement No. PHY0120999.

## Appendix A: Relaxation parameter and phase singularities

The large dimensional minmax problem (Eq. 17) can be expressed in a dual form:

$$\begin{cases} \min_{\rho_s} \varepsilon_m^2(\rho) = \min_{\rho_s} ||[I - P_m]\rho||^2 \\ \min_{\rho_s} \varepsilon_s^2(\rho) - \varepsilon_m^2(\rho) = \min_{\rho_s} 2\langle P_m \rho | \rho \rangle_r + c \end{cases} \quad (\text{A1})$$

The upper optimization is similar to the problem treated in Section 2, converging to a local minimum with a simple projected gradient method. The lower function, however, can be discontinuous in the presence of zeros ( $\tilde{\rho}_s = 0$ ) in Fourier space:

$$\langle \tilde{P}_m \tilde{\rho} | \tilde{\rho} \rangle = \sum \sqrt{I} |\tilde{\rho}_s + \tilde{\rho}_s| \quad (\text{A2})$$

which is a non-smooth v-shaped function of  $\tilde{\rho}_s$  for  $\tilde{\rho}_s = 0, \sqrt{I} > 0$ , and simple gradient methods oscillate around minima. The projected gradient step can be overestimated and requires the relaxation parameter  $\tilde{\beta}$ . Zeros in Fourier space are candidates (necessary but not sufficient condition) for the location of phase vortices, phase discontinuities, which are known to cause stagnation<sup>29</sup>. Analytical<sup>30</sup>, statistical<sup>3,29,31</sup>, and deterministic<sup>28,32</sup> methods have been proposed to overcome such singularities.

## Appendix B: Two dimensional gradient and Hessian

The function  $\mathcal{L}$  in reciprocal space can be expressed as:

$$\begin{aligned} \mathcal{L}(\tilde{\rho}_s + \tilde{\rho}_s) &= ||[I - \tilde{P}_m](\tilde{\rho}_s + \tilde{\rho}_s)||^2 - ||\tilde{\rho}_s||^2 \quad (\text{B1}) \\ &= \sum |\tilde{\rho}_s|^2 - 2\sqrt{I} |\tilde{\rho}_s + \tilde{\rho}_s| + \sqrt{I}. \end{aligned}$$

and the two components of the gradients:

$$\begin{aligned} \nabla \mathcal{L} &= 2 \begin{pmatrix} P_s \nabla \mathcal{L} \\ P_s \nabla \mathcal{L} \end{pmatrix} = 2 \begin{pmatrix} P_s [I - P_m](\rho_s + \rho_s) \\ -P_s P_m(\rho_s + \rho_s) \end{pmatrix} \quad (\text{B2}) \\ \nabla_s \mathcal{L} &= 2P_s [I - P_m](\rho_s + \rho_s) \\ \nabla_{\underline{s}} \mathcal{L} &= -2P_{\underline{s}} P_m(\rho_s + \rho_s). \end{aligned}$$

The corresponding steps  $\Delta \rho_s = -\frac{1}{2} \nabla_s \mathcal{L}$ ,  $\Delta \rho_{\underline{s}} = +\frac{1}{2} \nabla_{\underline{s}} \mathcal{L}$ .

The function  $\psi(\alpha, \beta)$  can be calculated in reciprocal space, provided that the components  $\tilde{\rho}_{s,\underline{s}}, \Delta \tilde{\rho}_{s,\underline{s}}$  are

known:

$$\begin{aligned} \psi(\alpha, \beta) &= ||[I - \tilde{P}_m](\tilde{\rho} + \alpha \Delta \tilde{\rho}_s + \beta \Delta \tilde{\rho}_{\underline{s}})||^2 \\ &- ||\tilde{\rho}_s + \beta \Delta \tilde{\rho}_{\underline{s}}||^2 \\ &= \sum_{\mathbf{k}} \left| |\tilde{\rho} + \alpha \Delta \tilde{\rho}_s + \beta \Delta \tilde{\rho}_{\underline{s}}| - \sqrt{I} \right|^2 \\ &- |\tilde{\rho}_s + \beta \Delta \tilde{\rho}_{\underline{s}}|^2 \\ &= \sum_{\mathbf{k}} I + |\tilde{\rho}_s + \alpha \Delta \tilde{\rho}_s|^2 \\ &- 2\sqrt{I} |\tilde{\rho} + \alpha \Delta \tilde{\rho}_s + \beta \Delta \tilde{\rho}_{\underline{s}}| \end{aligned} \quad (\text{B3})$$

Using common derivative rules:

$$\frac{\partial}{\partial x} |x| = \frac{x}{|x|}, \quad (\text{B4})$$

$$\frac{\partial}{\partial \alpha} |x + \alpha \Delta x| = \frac{\Re(\Delta x^\dagger (x + \alpha \Delta x))}{|x + \alpha \Delta x|}, \quad (\text{B5})$$

$$\frac{\partial}{\partial \alpha} \frac{x + \alpha \Delta x}{|x + \alpha \Delta x|} = \frac{\Delta x}{|x + \alpha \Delta x|} - \frac{x + \alpha \Delta x}{|x + \alpha \Delta x|^2} \cdot \frac{\Re(\Delta x^\dagger (x + \alpha \Delta x))}{|x + \alpha \Delta x|^2}, \quad (\text{B6})$$

$$\frac{\partial}{\partial \alpha} |x + \alpha \Delta x|^2 = 2\Re(\Delta x^\dagger (x + \alpha \Delta x)), \quad (\text{B7})$$

$$\frac{\partial^2}{\partial \alpha^2} |x + \alpha \Delta x| = \frac{|\Delta x|^2}{|x + \alpha \Delta x|} - \frac{\Re(\Delta x^\dagger (x + \alpha \Delta x))^2}{|x + \alpha \Delta x|^3}, \quad (\text{B8})$$

$$\frac{\partial^2}{\partial \alpha^2} |x + \alpha \Delta x|^2 = |\Delta x|^2, \quad (\text{B9})$$

and

$$\begin{aligned} \frac{\partial^2 |x + \alpha \Delta x + \beta \Delta y|}{\partial \alpha \partial \beta} &= \frac{\Re(\Delta x^\dagger \Delta y)}{|x + \alpha \Delta x + \beta \Delta y|} \\ &- \frac{\Re(\Delta x^\dagger (x + \alpha \Delta x + \beta \Delta y))}{|x + \alpha \Delta x + \beta \Delta y|^2} \\ &\cdot \frac{\Re(\Delta y^\dagger (x + \alpha \Delta x + \beta \Delta y))}{|x + \alpha \Delta x + \beta \Delta y|^2}, \end{aligned} \quad (\text{B10})$$

we can calculate the analytic expression for the gradient and Hessian. The gradient components (writing  $\tilde{\rho}_\tau = \tilde{\rho} + \tau^T \Delta \tilde{\rho} = \tilde{\rho} + \alpha \Delta \tilde{\rho}_s + \beta \Delta \tilde{\rho}_{\underline{s}}$ ) are:

$$\nabla_t \psi = 2 \langle \Delta \tilde{\rho} | [\tilde{P}_s - \tilde{P}_m] \tilde{\rho}_\tau \rangle_r, \quad (\text{B11})$$

$$\frac{\partial \psi}{\partial \alpha} = 2 \langle \Delta \tilde{\rho}_s | [I - \tilde{P}_m] \tilde{\rho}_\tau \rangle_r,$$

$$\frac{\partial \psi}{\partial \beta} = 2 \langle \Delta \tilde{\rho}_{\underline{s}} | [-\tilde{P}_m] \tilde{\rho}_\tau \rangle_r,$$

and the Hessian can be computed using  $\tilde{P}_m \tilde{\rho} = \frac{\tilde{\rho}}{|\tilde{\rho}|} \sqrt{I}$ . Starting from the simplest component:

$$\begin{aligned} \frac{\partial^2 \psi}{\partial \beta^2} &= -2 \left\langle \Delta \tilde{\rho}_{\underline{s}} \left| \frac{\partial \tilde{P}_m \tilde{\rho}_\tau}{\partial \beta} \right. \right\rangle \quad (\text{B12}) \\ &= 2 \sum -\frac{|\Delta \tilde{\rho}_{\underline{s}}|^2 \sqrt{I}}{|\tilde{\rho}_\tau|} + \frac{\Re(\Delta \tilde{\rho}_{\underline{s}}^\dagger \tilde{\rho}_\tau)^2 \sqrt{I}}{|\tilde{\rho}_\tau|^3} \\ &= 2 \sum -\frac{|\Delta \tilde{\rho}_{\underline{s}}|^2 \sqrt{I}}{|\tilde{\rho}_\tau|} + \frac{\sqrt{I}}{2|\tilde{\rho}_\tau|} \frac{\Re(\Delta \tilde{\rho}_{\underline{s}}^\dagger \tilde{\rho}_\tau)(\Delta \tilde{\rho}_{\underline{s}}^\dagger \tilde{\rho}_\tau + \Delta \tilde{\rho}_{\underline{s}} \tilde{\rho}_\tau^\dagger)}{|\tilde{\rho}_\tau|^2} \\ &= 2 \left\langle \Delta \tilde{\rho}_{\underline{s}} \left| -\frac{\sqrt{I}}{2|\tilde{\rho}_\tau|} \left( 1 - \frac{\tilde{\rho}_\tau^2}{\Delta \tilde{\rho}_{\underline{s}}^2} \frac{|\Delta \tilde{\rho}_{\underline{s}}|^2}{|\tilde{\rho}_\tau|^2} \right) \right| \Delta \tilde{\rho}_{\underline{s}} \right\rangle_r, \end{aligned}$$

$$\begin{aligned}
\frac{\partial^2 \psi}{\partial \alpha^2} &= 2 \left\langle \Delta \tilde{\rho}_s \left| \frac{\partial [\mathbf{I} - \tilde{\mathbf{P}}_m] \tilde{\rho}_\tau}{\partial \alpha} \right\rangle_r, \\
&= 2 \sum |\Delta \tilde{\rho}_s|^2 - \frac{|\Delta \tilde{\rho}_s|^2 \sqrt{I}}{|\tilde{\rho}_\tau|} + \frac{\Re(\Delta \tilde{\rho}_s^\dagger \tilde{\rho}_\tau)^2 \sqrt{I}}{|\tilde{\rho}_\tau|^3} \\
&= 2 \left\langle \Delta \tilde{\rho}_s \left| \left[ 1 - \frac{\sqrt{I}}{2|\tilde{\rho}_\tau|} \left( 1 - \frac{\tilde{\rho}_\tau^2}{\Delta \tilde{\rho}_s^2} \frac{|\Delta \tilde{\rho}_s|^2}{|\tilde{\rho}_\tau|^2} \right) \right] \right| \Delta \tilde{\rho}_s \right\rangle_r
\end{aligned} \tag{B13}$$

The cross terms:

$$\begin{aligned}
\frac{\partial^2 \psi}{\partial \beta \partial \alpha} &= 2 \left\langle \Delta \tilde{\rho}_s \left| \frac{\partial [\mathbf{I} - \tilde{\mathbf{P}}_m] \tilde{\rho}_\tau}{\partial \beta} \right\rangle \right. \\
&= 2 \left\langle \Delta \tilde{\rho}_s \left| -\frac{\sqrt{I}}{2|\tilde{\rho}_\tau|} \left( 1 - \frac{\tilde{\rho}_\tau^2}{\Delta \tilde{\rho}_s^2} \frac{|\Delta \tilde{\rho}_s|^2}{|\tilde{\rho}_\tau|^2} \right) \right| \Delta \tilde{\rho}_s \right\rangle_r \\
&= 2 \left\langle \Delta \tilde{\rho}_s \left| -\frac{\sqrt{I}}{2|\tilde{\rho}_\tau|} \left( 1 - \frac{\tilde{\rho}_\tau^2}{\Delta \tilde{\rho}_s^2} \frac{|\Delta \tilde{\rho}_s|^2}{|\tilde{\rho}_\tau|^2} \right) \right| \Delta \tilde{\rho}_s \right\rangle_r.
\end{aligned} \tag{B14}$$

## References

1. J. Miao, P. Charalambous, J. Kirz, D. Sayre, *Nature* **400**, 342 (1999).
2. D. Shapiro, P. Thibault, T. Beetz, V. Elser, M. Howells, C. Jacobsen, J. Kirz, E. Lima, H. Miao, A. Neiman, D. Sayre, *PNAS* **102** (43), 1543 (2005).
3. J. Miao, C-C. Chen, C. Song, Y. Nishino, Y. Kohmura, T. Ishikawa, D. Ramunno-Johnson, T-K. Lee, and S. H. Risbud, *Phys. Rev. Lett.* **97**, 215503 (2006)
4. M. A. Pfeifer, G. J. Williams, I. A. Vartanyants, R. Harder & I. K. Robinson, *Nature* **442**, 63-67 (2006).
5. A. Barty et al., "Three-dimensional ceramic nanofoam lattice structure determination using coherent X-ray diffraction imaging: insights into deformation mechanisms", submitted.
6. H. N. Chapman, A. Barty, S. Marchesini, A. Noy, C. Cui, M. R. Howells, R. Rosen, H. He, J. C. H. Spence, U. Weierstall, T. Beetz, C. Jacobsen, D. Shapiro, *J. Opt. Soc. Am. A* **23**, 1179-1200 (2006), arXiv:physics/0509066.
7. H. N. Chapman, A. Barty, M. J. Bogan, S. Boutet, M. Frank, S. P. Hau-Riege, S. Marchesini, B. W. Woods, S. Bajt, W. H. Benner, R. A. London, E. Plönjes, M. Kuhlmann, R. Treusch, S. Düterer, T. Tschentscher, J. R. Schneider, E. Spiller, T. Möller, C. Bostedt, M. Hoener, D. A. Shapiro, K. O. Hodgson, D. Van Der Spoel, F. Burmeister, M. Bergh, C. Caleman, Gösta Huldt, M. M. Seibert, F. R. N. C. Maia, R. W. Lee, A. Szöke, N. Timneanu, Janos Hajdu, *Nature Physics* **2**, 789-862 (2006), [arxiv:physics/0610044].
8. P. W. Hawkes & J. C. H. Spence (Eds.), *Science of Microscopy* (Springer, 2007).
9. J. R. Fienup, *Opt. Lett.* **3**, 27-29 (1978).
10. J. R. Fienup, *Appl. Opt.* **21**, 2758-2769 (1982).
11. A. Levi and H. Stark, *J. Opt. Soc. Am. A* **1**, 932-943 (1984).
12. H. Stark, *Image Recovery: Theory and applications* (Academic Press, 1987).
13. V. Elser, *J. Opt. Soc. Am. A* **20**, 40-55 (2003).
14. H. H. Bauschke, P. L. Combettes, and D. R. Luke, *J. Opt. Soc. Am. A* **19**, 1334-1345 (2002).
15. H. H. Bauschke, P. L. Combettes, and D. R. Luke, *J. Opt. Soc. Am. A* **20**, 1025-1034 (2003).
16. D. R. Luke, *Inverse Problems* **21**, 37-50 (2005), (arXiv:math.OA/0405208).
17. V. Elser, I. Rankenburg, and P. Thibault, "Searching with iterated maps". *Proc. Nat. Acc. Sci.* **104**, 418-423 (2007).
18. S. Marchesini, *Rev. Sci. Instr.* **78**, 011301 (2007), (arXiv:physics/0603201).
19. S. Marchesini et al. *Phys. Rev. B* **68**, (2003) 140101(R), (arXiv:physics/0306174).
20. D. R. Luke, J. V. Burke, R. G. Lyon, *SIAM Review* **44**, 169-224 (2002).
21. R. Gerchberg and W. Saxton, *Optik* **35**, 237-246 (1972).
22. M. R. Hestenes, *Conjugate Direction Methods in Optimization*, (Springer-Verlag, 1980).
23. W. H. Press, S. A. Teukolsky, W. T. Vetterling and B. P. Flannery, *Numerical Recipes in C* (Cambridge University Press, 1992).
24. M. J. D. Powell, *Lecture Notes in Mathematics* **1066**, 122-141 (1984).
25. E. Polak, *Computational Methods in Optimization* (Academic Press, 1971).
26. R. Fletcher, *Practical Methods of Optimization* (John Wiley & Sons, 2000).
27. J. Nocedal, S. J. Wright, *Numerical Optimization* (Springer Verlag, 2006).
28. G. Oszlányi and A. Süto, *Acta Cryst.* **A61**, 147-152 (2005).
29. J. R. Fienup, C. C. Wackerman, *J. Opt. Soc. Am. A* **3**, 1897-1907 (1986).
30. P-T. Chen, M. A. Fiddy, C-W. Liao and D. A. Pommet, *J. Opt. Soc. Am. A* **13**, (1996), 1524-31.
31. S. Marchesini, H. N. Chapman, A. Barty, M. R. Howells, J. C. H. Spence, C. Cui, U. Weierstall, and A. M. Minor, *IPAP Conf. Series* **7**, 380-382 (2006), (arXiv:physics/0510033).
32. T. Isernia, G. Leone, R. Pierri, and F. Soldovieri, *J. Opt. Soc. Am. A* **16**, 1845-1856 (1999).